

Local Particle Transport Diagnostics in Plasma Edge Using Tracer-Encapsulated Solid Pellet Injection

TAMURA Naoki*, KHLOPENKOV Konstantin¹⁾, SUDO Shigeru¹⁾,
VINIAR Igor²⁾, SERGEEV Vladimir^{1),2)} and LHD Experimental Group¹⁾
Grad. Univ. Advanced Studies, Oroshi-cho 322-6, Toki 509-5292, Japan

¹⁾ *National Institute for Fusion Science, Oroshi-cho 322-6, Toki 509-5292, Japan*

²⁾ *State Technical University of St. Petersburg, Polytechicheskaya 29, St. Petersburg 195251, Russia*

(Received: 5 December 2000 / Accepted: 27 August 2001)

Abstract

For an accurate measurement of local particle transport, tracer-encapsulated solid pellet (TESPEL) has been developed. TESPEL consists of polystyrene $(-\text{CH}(\text{C}_6\text{H}_5)\text{CH}_2-)_n$ as an outer shell and tracer particles as an inner core. The essential point of this method is based upon the production of a both poloidally and toroidally localized particle source as tracers, which are deposited at first within a very small volume in the plasma. To clarify the particle transport property, especially under the influence of the radial electric field, the radial diffusion of these tracer ions will be detected by means of charge exchange recombination spectroscopy (CXRS) array at the location of a neutral beam. The TESPEL injection has been accomplished successfully for the LHD plasma, and the very local deposition of tracers was confirmed by the CCD images of ablating TESPEL and also by the high time-resolved observation of the ablation lights from TESPEL.

Keywords:

impurity injection, tracer-encapsulated solid pellet (TESPEL), local particle transport, tracer particles, local particle deposition

1. Introduction

The study of particle transport in magnetically confined plasma is still one of the important issues from the viewpoint of designing an experimental device or a fusion reactor. This work has been done intensely by means of impurity pellet injection and laser blow-off method [1,2]. However, these conventional methods have essential disadvantages, such as a broad source profile of the injected impurities and the opacity of the total amount of the impurity particles. To solve these problems and promote particle transport studies, a tracer-encapsulated cryogenic pellet (TECPEL) has been proposed [3]. The essential point of this method is based

upon the production of a both poloidally and toroidally localized particle source as tracers, which is deposited at first within a small volume in the plasma. The locally deposited "tracer" particles will be ionized immediately by a bulk plasma and move along the lines of magnetic field at first. Subsequently these tracers will diffuse toward the radial direction. Such a behavior of tracers in both directions will make diagnostics of particle transport much clearer because of the narrow distribution of the impurity particles. Moreover, the total amount of the deposited tracer particles can be identified clearly, since the size of the inner core of TECPEL is known.

*Corresponding author's e-mail: ntamura@LHD.nifs.ac.jp

2. Experimental Apparatus

TECPEL injector and the associated system have been substantially developed. However, for a start, a tracer-encapsulated solid pellet (TESPEL), which has been developed on Compact Helical System (CHS), was applied to the Large Helical Device (LHD). The TESPEL injection system has been installed on LHD in 1999. TESPEL is based on the same concept as TECPEL, but the outer part of TESPEL is made of polystyrene ($-\text{CH}(\text{C}_6\text{H}_5)\text{CH}_2-$) $_n$, while that of TECPEL is made of frozen hydrogen as an outer shell. Therefore, TESPEL can be handled conveniently at the room temperature. The fabrication method of TESPEL is described in detail in ref. [4]. The current typical outer and inner diameters of the polystyrene shell are 700–900 μm and 200 μm , respectively. As a tracer, LiH and Si were used so far.

The TESPEL injection system consists of a TESPEL injector and a differential pumping system with three expansion chambers isolated by fast gate-valves. The TESPEL injector consists of magazine with a rotating disk, gun barrel with 41 cm long and an inner diameter of 1.0 mm and observation chamber. The rotating disk has 60 holes with an inner diameter of 0.99 mm for holding TESPELs. In one series of experiments, 59 pellets can be loaded in the disk. The AC servomotor, which can be controlled remotely, is connected to the disk, and rotates the disk to position precisely the next TESPEL on the injection axis. This action will be finished within an interval of discharges with 3 minutes cycle. The TESPEL injector is connected to the 1st expansion chamber through the gun barrel. This 1st expansion chamber is connected to a buffer tank (volume: 100 l) to consume the pressure jump due to the propellant gas. And the 2nd and 3rd expansion chambers are evacuated by the turbo molecular pump (TMP). These TMPs have been installed at about 6 m away from the connecting port with LHD, for avoiding an effect from the high magnetic field. The ultimate pressure at the 3rd expansion chamber is 1.0×10^{-5} Pa. The schematic of TESPEL injector system and the associated diagnostic system are shown in Fig. 1. In Fig. 1, LiH as a tracer particle is considered. Two He-Ne lasers and light detectors have been installed as the light barrier at the each observation window of the 1st and 3rd expansion chamber. The distance between these barriers is 3.22 m, thus we can estimate roughly the TESPEL velocity from the time difference of the TESPEL crossing the light barrier. The ablation emission of TESPEL injected into a LHD plasma is observed by the

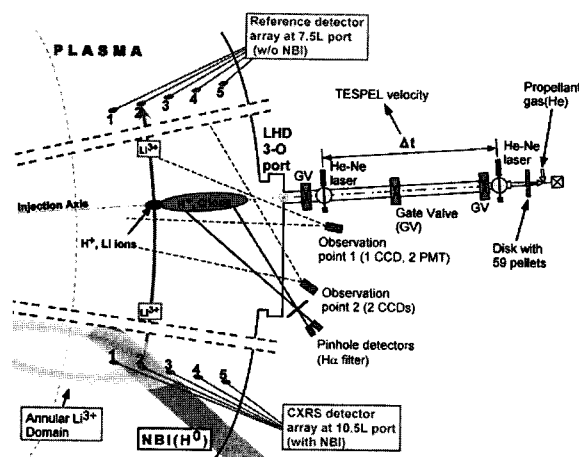


Fig. 1 The schematic of TESPEL injector system and the associated diagnostics system. Here, LiH as a tracer particle is considered.

CCD camera directly and by two photo multiplier tubes (PMT), on the back to the direction along the injection axis (Observation point 1 in Fig. 1). These CCD cameras and PMTs are equipped with the interference filter. The image of this CCD camera provides the information about the deviation angle of the TESPEL flight path from the TESPEL injection axis. The additional two compact CCD cameras have been installed at the location for looking aslope at the TESPEL injection axis (Observation point 2 in Fig. 1). From the light intensity profile in these two CCD images, the deposited location of the tracer particles in a LHD plasma is obtained. In order to obtain the TESPEL velocity in the plasma, the two light detectors using a pinhole slit have been installed at the same location of these CCD cameras.

The Large Helical Device (LHD) [5] is a large Heliotron device (poloidal period number $l = 2$, and toroidal period number $m = 10$) with a major radius $R = 3.55\text{--}3.75$ m, an average minor radius $r = 0.6$ m, magnetic field up to 3 T by superconducting coils. The electron density (n_e) profiles are measured with a multi-chord FIR laser interferometer [6].

3. Experimental Results

3.1 TESPEL Velocity and the Penetration Depth

TESPEL is accelerated by a high-pressure helium gas. Figure 2 shows the TESPEL size dependence of the TESPEL velocity with the propellant gas pressure of 20 bar (open circles) and 25 bar (closed squares). In case

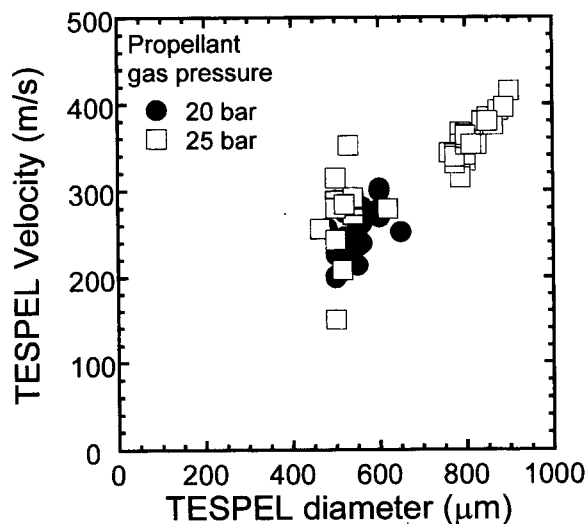


Fig. 2 The dependence of the TESPEL velocity on the TESPEL diameter with the propellant gas pressure of 20 bar (closed circles) and 25 bar (open squares).

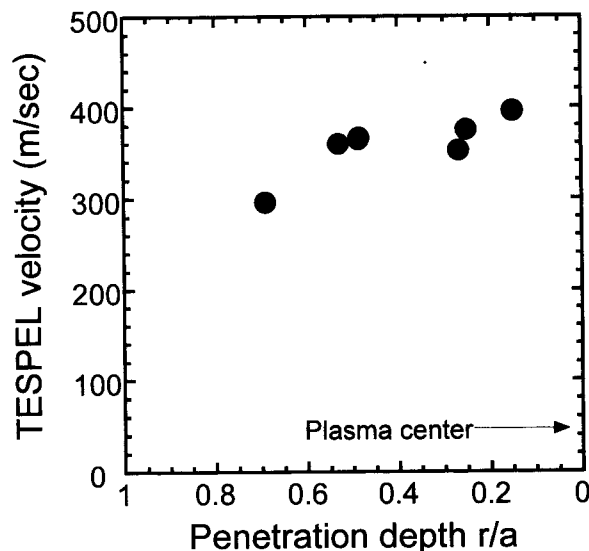


Fig. 3 The dependence of the TESPEL diameter on the penetration depth in r/a with a fixed line averaged density ($n_e \sim 4.0 \times 10^{19} \text{ m}^{-3}$).

that TESPEL diameter was 500–600 μm , the TESPEL velocity in the range of 200–300 m/s was obtained almost independently of the propellant gas pressure. On the other hand, in case of TESPEL size in range of $\phi 800\text{--}900 \mu\text{m}$, the TESPEL velocity in the range of 300–400 m/s is obtained. This can be explained as follows. TESPEL is accelerated by a gas in the gun barrel caused by opening the fast valve. But in case that TESPEL diameter is smaller than the inner diameter of the gun barrel, that gas flow cannot accelerate TESPEL efficiently, since the gas flow can pass through the gap between the inner wall of the gun barrel and TESPEL. On the other hand, as Fig. 2 indicates, when that size came to be close to the inner diameter of the gun barrel, TESPEL would be accelerated efficiently and its velocity would show the evident dependence on its own size. The dependence of the TESPEL size with a fixed line averaged density ($n_e \sim 4.0 \times 10^{19} \text{ m}^{-3}$) on the penetration depth is shown in Fig. 3. Since the TESPEL velocity is obviously in proportion to that size over the $\phi 800 \mu\text{m}$ TESPEL, the dependence of that velocity on the penetration depth might have the almost same property as on that size. The deepest penetration depth of $r/a = 0.15$ was obtained with the diameter with $\phi 900 \mu\text{m}$ and the velocity with 395.5 m/sec. Thus, the deposition of the tracer particles in the core region of a LHD plasma is expected by using TESPEL of more than $\phi 900 \mu\text{m}$. Consequently, by selecting the optimum TESPEL size, any location can be predetermined for the local

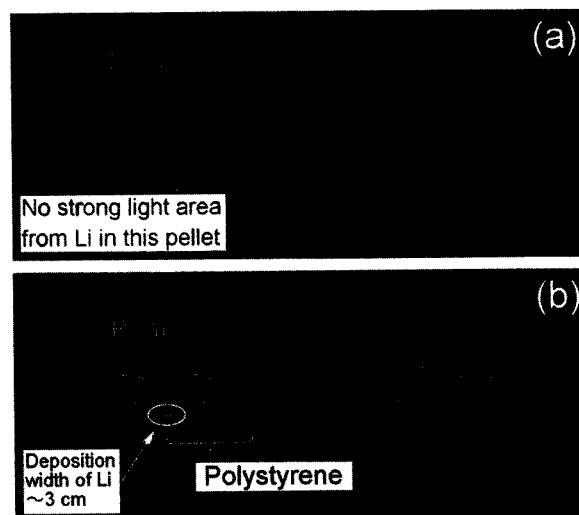


Fig. 4 CCD images of the ablating TESPEL through a Li I filter ($\lambda = 671.3 \text{ nm}$, $\delta\lambda = 3.6 \text{ nm}$) in case (a) without tracer particles (LiH) of TESPEL and (b) with those of TESPEL.

deposition of tracer particles.

3.2 Observation of Local Deposition of Tracer Particles

The CCD images of the ablating TESPEL through a Li I filter (a) without tracer particles (LiH) and (b) with those in a pellet are shown in Fig. 4. In Fig. 4(b), a

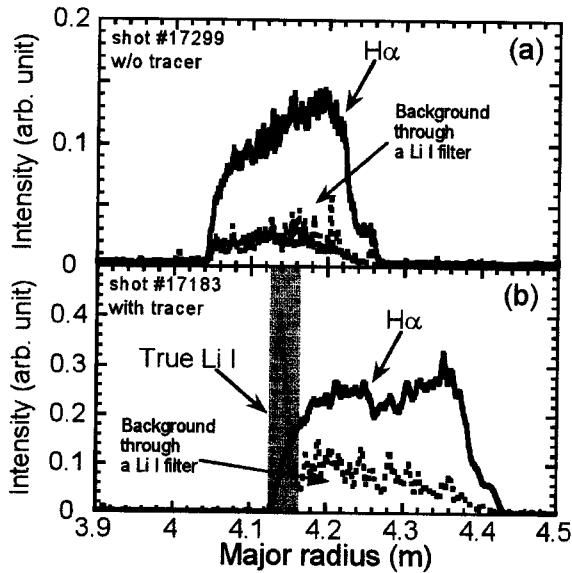


Fig. 5 $H\alpha$ (solid curve) and Li I (dotted curve) emission from the ablation cloud of TESPEL as a function of major radius, which is calculated from the TESPEL velocity. (a) Without tracer particles (LiH) of TESPEL and (b) with those of TESPEL.

strong light emission is seen at the left edge of the filament. This intense luminescence can be considered to be due to the Li ions. Another part of the filament is attributed to a background light through a Li I filter with bandwidth 3.6 nm. Figure 5 shows $H\alpha$ (solid curve) and Li I (dotted curve) emission from the ablation cloud of TESPEL as a function of major radius, which was calculated from the TESPEL velocity. In case of Fig. 5(a), TESPEL without the tracer particles was injected, and in case of Fig. 5(b), TESPEL with those was injected. While almost no significant light emission through a Li I filter was observed in Fig. 5(a), the sharp increase in the final phase of the ablation process was observed in Fig. 5(b). From the obtained TESPEL velocity, the deposition width was calculated as 3 cm. This deposition width is in good agreement with the CCD image.

3.3 Observation of Behavior of the Tracer Particles

The tracer particles, deposited locally, diffuse in the plasma. In case of LiH tracer, this diffusion, especially to the radial direction, is measured by observing the Li^{2+} lights (λ : 449.9 nm) arising from the process of charge exchange of Li^{3+} ions with neutral hydrogen atoms, originated from neutral beam injection (NBI) as shown in Fig. 1. To obtain the pure emission from the charge exchange process in the core region, the Li^{2+} lights are

observed at the location with NBI path and at that without NBI path, and the difference of these signal is used as a pure emission from the core region. In the 3rd campaign of LHD experiment, the measurement of the radial diffusion of Li had been tried, but the intensity from such tracer ions was not enough for obtaining the diffusion property. The other and higher Z materials (e.g. Si) can be used for obtaining the better intensity.

4. Discussions

Generally speaking, the property of the radial particle transport is expected to be highly correlated with the radial electric field (E_r). The improvement of ion transport, induced by the transition of E_r from negative value (ion root) to positive one (electron root), is predicted by the neoclassical transport theory [7]. In LHD, the radial electric field is derived from the poloidal and toroidal rotation velocity and pressure gradient of Neon impurity measured with charge exchange spectroscopy [8] and such a transition of E_r near the plasma edge was observed under the condition of the NBI heating for the first time [9]. Moreover in [9], it is indicated that, in case of the discharges with ice pellet injection, the large E_r shear even with negative E_r region might generate the improvement of ion confinement.

For each phenomenon, E_r transition and E_r shear, the peripheral region ($\rho > 0.8$) is of critical importance region. According to the previous chapter, by using TESPEL with around $\phi 300 \mu\text{m}$, the well-defined source of impurity can be created just inside or in such a region. The transition of E_r under the condition of the NBI heating was observed at the low $n_e \sim 7.0 \times 10^{18} \text{ m}^{-3}$ at $R_{ax} = 3.75 \text{ m}$ and $3.0 \times 10^{18} \text{ m}^{-3}$ at $R_{ax} = 3.6 \text{ m}$. The resultant electron density jump by the injection of TESPEL with $\phi 300 \mu\text{m}$ is expected up to $0.16 \times 10^{18} \text{ m}^{-3}$. Since this relatively small density jump might be not enough to cause the undesirable transition from electron root to ion root due to the increase of density, the clear and incomparable characteristics of ion "particle" transport for the discharges with the E_r transition will be obtained and compared with the neoclassical transport theory by using TESPEL injection. Consequently, our diagnostic method will be surely powerful tool for clarifying directly the improvement of ion transport, that is, the improvement of "ion confinement", especially under the influence of the radial electric field near the plasma edge.

Acknowledgments

This work was supported partly by grant No.

L00537 of Japan Society for the Promotion of Science.

References

- [1] H. Kaneko *et al.*, Nucl. Fusion. **27**, 1075 (1987).
- [2] K. Khlopenkov *et al.*, Fusion Engineering and Design. **34-35**, 337 (1997).
- [3] S. Sudo, J. Plasma Fusion Res. **69**, 1349 (1993).
- [4] K. Khlopenkov *et al.*, Rev. Sci. Instrum. **69**, 319 (1998).
- [5] M. Fujiwara *et al.*, Nucl. Fusion **40**, 1157 (2000).
- [6] K. Kawahata *et al.*, Rev. Sci. Instrum. **70**, 707 (1999).
- [7] Y. Ogawa *et al.*, Nucl. Fusion. **32**, 119 (1992).
- [8] K. Ida *et al.*, Rev. Sci. Instrum. **71**, 2360 (2000).
- [9] K. Ida *et al.*, National Institute for Fusion Science Research Report NIFS-655, Japan (2000).